Phys Chem Minerals (2003) 30: 353–365
DOI 10.1007/s00269-003-0320-8

ORIGINAL PAPER

I. P. Swainson · M. T. Dove · D. C. Palmer

Infrared and Raman spectroscopy studies of the α–β phase transition in cristobalite

Received: 9 July 2002 / Accepted: 12 March 2003

Abstract Infrared and Raman spectra of cristobalite are presented as a function of temperature through the phase transition. The modes are assigned and the assignments compared to those of earlier workers. The compatibility of modes at the Γ-point of the α-phase with the X and Γ-points of the β-phase is given. In the transition region of ca. 500–550 K, smooth changes in intensity, frequency and linewidths are seen in many modes, indicative of coexistence of α- and β-forms.

Keywords Cristobalite · Silica · Infrared · Raman · Mode assignment · Phase transition

Introduction

Cristobalite is the thermodynamically stable phase of silica above 1743 K and, like quartz, its structure consists of an infinite, three-dimensional framework of corner-bonded tetrahedra. Because the reconstructive transitions to tridymite and quartz are so slow, cristobalite exists in a metastable state below 1743 K. At ambient pressures cristobalite undergoes a highly discontinuous structural phase transition at $T_{tr} \approx 540$ K, but the precise temperature of this transition is strongly dependent on the sample history. The high-temperature β-phase has cubic symmetry, $Fd3m$ (O_h^7), and the low-temperature α-phase is tetragonal, $P4_12_12$ (D_4^4) (Schmahl et al. 1992). The volume of the α-phase is roughly half that of the β-phase, consistent with a zone boundary instability. Moreover, there is a large difference in the value of T_{tr} on heating and cooling, and a temperature interval where both phases coexist, making the definition of a sharp transition temperature difficult.

A number of recent papers have been concerned with the phase transition in cristobalite. These include the papers of Hatch and Ghose (1991), Schmahl et al. (1992) and Swainson and Dove (1993a,b, 1995) mentioned above. In addition, NMR studies (Spearing et al. 1992; Phillips et al. 1993) and electron diffraction studies (Hua et al. 1988; Welberry et al. 1989; Withers et al. 1989) have been reported.

Several early papers were written on the Raman and infrared (IR) spectra of cristobalite, but most of the spectra were taken at isolated temperatures, e.g., Simon and McMahon (1953), Gaskell (1967) and Plendl et al. (1967). Later spectroscopic studies (Bates 1972; Etchepare et al. 1978; Cherukuri et al. 1985) were mostly concerned with mode assignment at room temperature, although Bates (1972) presented results of Raman scattering experiments at several temperatures, including temperatures in the β-phase. Hua et al. (1989) performed detailed lattice dynamics calculations, determined the eigenvectors of the normal modes of β-cristobalite, and also reviewed mode assignments in the IR and Raman. Finnie et al. (1994) reported variable temperature IR emission spectra of cristobalite and related compounds. A study of the pressure dependence of the Raman spectra of α-cristobalite and the transition to the high-pressure phase was reported by Palmer et al. (1994). This has also been studied by diffraction by Dove et al. (2000).

In this paper we present a combined analysis of variable temperature IR absorption and Raman scattering spectra of powdered cristobalite in much finer detail than has been published before at temperatures

I. P. Swainson (✉)
Neutron Program for Materials Research, SIMS,
National Research Council of Canada, Chalk River Laboratories,
Chalk River, Ontario, K0 J 1J0, Canada
e-mail: Ian.Swainson@nrc.ca
Tel.: +1 613 584 8811 ext 3995
Fax: +1 613 584 4040

M. T. Dove
Department of Earth Sciences, University of Cambridge,
Downing Street, Cambridge CB2 3EQ, UK

D. C. Palmer
Department of Earth Sciences, The Open University,
Walton Hall, Milton Keynes, MK7 6AA, UK

Present address: CrystalMaker Software,
P.O. Box 183, Bicester, Oxfordshire, OX26 3TA, UK

from 5 to 600 K. We also present a symmetry analysis of the IR- and Raman-active modes and compare it to those of earlier workers. This symmetry analysis incorporates the full decomposition at the Γ-point of α-cristobalite and the Γ- and *X*-points of β-cristobalite. As the *X*-point is the soft zone boundary point governing the α–β transition in cristobalite; this allows one to map all Γ-point modes in α-cristobalite to Γ- and *X*-modes in β-cristobalite.

In the text we will refer to the different modes by their frequency at low temperature with their symmetry in parentheses. In some cases we will also include the corresponding symmetry in the high-temperature β-phase. In the few cases where there is any ambiguity in the symmetry of a mode in either phase, the possible symmetries will be displayed by a "/". For example, the mode at 276 cm^{-1} has *E* symmetry in the α-phase and X_1 or X_2 symmetry in the β-phase, and we will write it as either 276 cm^{-1} (*E*) or 276 cm^{-1} ($E \leftrightarrow X_1/X_2$).

Spectroscopy and phase transitions

Soft modes

There are two principal effects of a structural phase transition on the spectra observed in an IR absorption or Raman scattering experiment. The first is the occurrence of a soft mode, which is seen as one or more mode frequency that falls to zero at the transition temperature of a second-order phase transition, or which tends towards zero for a first-order phase transition. The softening of the mode frequency implies a softening of the restoring force against a corresponding static distortion of the structure. On cooling below the transition temperature the soft mode will increase in frequency. Soft modes are generally associated with phase transitions that are in the displacive limit, where there are long-range correlated atomic motions. Although soft modes have been observed in association with many phase transitions in ionic materials, there have been hardly any observations of soft modes in aluminosilicates – quartz appears to be the only case where a soft mode has been unambiguously characterized in both phases (Shapiro et al. 1967; Dolino et al. 1992). In the case of cristobalite, if a soft mode exists in the β-phase, it has a wave vector on the surface of the Brillouin zone at (0,0,1), labelled as the *X*-point (Zak 1969). Due to the nature of Raman scattering and IR absorption, only modes at the zone centre can be measured, and therefore any soft mode will be observed only in the spectra of the α-phase.

Hard modes

Whereas many spectroscopic studies of structural phase transitions have focused on the search for soft mode behaviour, information may also be extracted from the temperature dependence of high-frequency modes, the so-called hard modes (Salje 1992). The theory of hard mode IR and Raman spectroscopy has been described in detail by Petzelt and Dvorak (1976a,b). A somewhat simpler description of hard mode behaviour has been given by one of us (Dove 1993; Dove et al. 1993).

It is often claimed that IR and Raman spectroscopy probe local interactions. This is because associated with any phonon mode is a coherence length, and for many hard modes the coherence length can be quite short. Because of this short coherence length, if β-cristobalite consisted of an average of domains of the α-phase, the phonon peaks that are symmetry-allowed in the α-phase should persist as sharp peaks in the Raman and IR spectra of the β-phase. For example, experiments on quartz have shown that modes that are not allowed to be IR-active according to the symmetry of the high-temperature phase disappear on heating above T_{tr}, indicating that the high-temperature phase is not simply an average over domains of the low-temperature phase (Salje et al. 1992). This point is not always fully appreciated, owing to the existence of a peak in the Raman spectra that persists in the high-temperature phase but which had been assigned a symmetry that should be Raman-inactive (Shapiro et al. 1967). The problem was resolved by recognising that this peak is actually a two-phonon peak that interacts with the soft mode (Scott 1968). There is recent evidence (Finnie et al. 1994) that at least one such two-phonon process is present in the spectra of cristobalite.

Rigid unit modes

General comments

Rigid unit modes (abbreviated RUMs) are normal modes that propagate without distortion of the SiO_4 tetrahedra (Vallade et al. 1992; Dove et al. 1992, 1993; Giddy et al. 1993; Dove et al. 1995; Hammonds et al. 1996), and subsequently can have relatively low frequencies. For this reason RUMs are natural candidates as soft modes for displacive phase transitions in silicates, and in quartz the role of the RUMs as soft modes has been analyzed in some detail both theoretically (Tautz et al. 1991; Vallade et al. 1992) and experimentally (Dolino et al. 1992).

The possible existence of low-frequency modes in a framework silicate may be seen to arise by the description of the network in terms of a model potential of the form (Thorpe 1983; Swainson and Dove 1993a):

$$V = \frac{1}{2}\sum_{\langle ij \rangle} \alpha_{ij} \Delta r_{ij}^2 + \frac{1}{2}\sum_{\langle ijk \rangle} \beta_{ijk} \Delta \vartheta_{ijk}^2 \quad , \tag{1}$$

where α_{ij} and β_{ijk} are the intratetrahedral Si–O bond-stretching and O–Si–O bond-bending force constants, respectively. In this model there are no intertetrahedral terms governing the Si–O–Si angle. Strong intratetrahedral restoring forces and negligible intertetrahedral

interactions lead to an approximation where the SiO_4 tetrahedra may be treated as rigid units whose mutual orientations are nearly independent. The concept of RUMs arises naturally from this approximation as residual degrees of freedom in the framework – the RUM solutions to the corresponding phonon equations will have exactly zero frequency (Thorpe 1983; Giddy et al. 1993; Swainson and Dove 1993a). While this model potential is very simple, in more realistic potentials RUMs become external modes that are low but not precisely zero in frequency.

Rigid unit modes in cristobalite

The set of RUMs in the β- and α-phases of cristobalite has been previously determined (Dove et al. 1992, 1993; Giddy et al. 1993) and are given in Tables 1 and 2. All crystals with a well-defined unit can be considered to have rigid unit modes at $\mathbf{k} = \mathbf{0}$ as the acoustic modes always move all the atoms in phase at this limit. What is of interest is the additional low-frequency optic modes in framework silicates which occur throughout the Brillouin Zone. Table 1 shows that there are RUMs for whole planes of wavevectors (Θ_2) in reciprocal space in the β-phase. The other lines and points are geometrical projections of these planes in the Brillouin zone. We have previously proposed that presence of so many RUMs in β-cristobalite causes phonon-induced dynamic disorder within the structure (Swainson and Dove 1993a). Infrared and Raman spectroscopy are both limited techniques, as they only give direct information about normal modes with wavevectors close to the zone centre ($\mathbf{k} = \mathbf{0}$). However, the presence of Θ_2 planes of RUMs in β-cristobalite has very strong experimental evidence in the form of the strong **k**-dependence of planes of diffuse scattering measured by TEM (Hua et al. 1988; Withers et al. 1989). The double-degenerate X_4 RUM at $\mathbf{k} = (0, 0, 1)$ has been identified as providing the instability for the phase transition (Hatch and Ghose 1991; Dove et al. 1992, 1993; Giddy et al. 1993; Swainson and Dove 1993a). One might loosely call this the soft mode, to the extent to which this concept is valid for disordered crystals. The lowering of the symmetry in the α-phase causes an increase in the number of independent constraints on the framework and hence the number of RUMs is reduced (Swainson and Dove 1993a). The plane of RUMs is reduced to a single line in α-cristobalite (see Table 2), corresponding to the one set of diffuse streaks seen in TEM diffraction patterns of this phase (Hua et al. 1988; Withers et al. 1989). We note that there are, in fact, more diffuse streaks than one could predict in α-cristobalite from the tabulation of pure RUMs of Table 2. In fact, additional low-frequency modes called quasi-RUMs or QRUMs also exist in many structures. Unlike true RUMs, these modes always include a minor amount of distortion of the tetrahedra and therefore have always have a low, finite frequency, even in idealized structures, which may cause diffuse scattering (Hammonds et al.1996; Pryde et al. 1996).

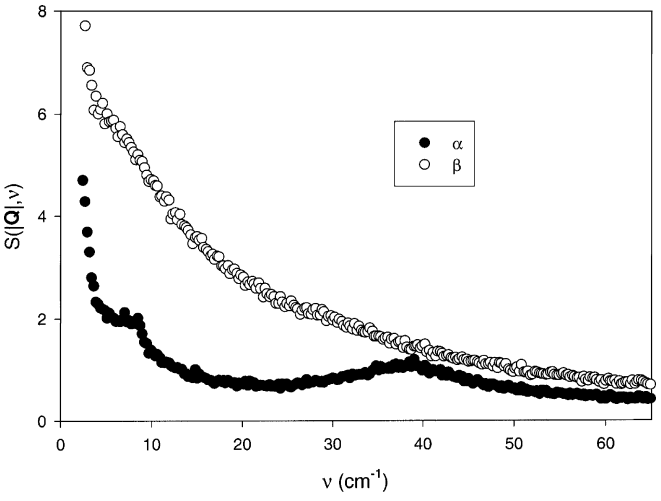

Fig. 1 TFXA spectrum of S(|**Q**|,ν) of α- and β-cristobalite, showing the dramatic increase in the number of low-frequency modes in the β-phase caused by the symmetry change

The change in the number of low-frequency modes caused by the symmetry change is demonstrated by a measurement of S(|**Q**|, ν) performed on powdered cristobalite with the instrument TFXA at the ISIS source, Rutherford Appleton Laboratory, UK. We use the symbol S(|**Q**|, ν), rather than S(**Q**, ν), the usual symbol for the scattering function or dynamic structure factor, because we are measuring parabolic |**Q**|-ν sections from a powder. As TFXA takes parabolic **Q**-ν sections the

Table 1 Rigid unit modes in β-cristobalite. Superscripts on the *left hand side* of the mode denote its degeneracy. The labelling of the representations at high-symmetry, non-zone-centre points is that of Zak (1969). The labelling of zone-centre representations is that of Mulliken (Mulliken 1933; Bradley and Cracknell 1972)

Wavevector	Rigid-unit mode
0,0,0 (Γ)	$T_{1u}^{a} + T_{2u}$
0,ξ,0 (Δ)	${}^2\Delta_3$
ξ,ξ,ξ (Λ)	${}^2\Lambda_3 + \Lambda_2$
ξ,ξ,0 (Σ)	Σ_2
½ ½ ½ (L)	$L_4 + L_2$
ξ,1, ξ (S)	S_2
0,1,0 (X)	${}^2X_4$
ξ,ξ,ζ (Θ)	Θ_2

[a] T_{1u} is an acoustic mode

Table 2 Rigid unit modes in α-cristobalite. Superscripts on *the left hand side* of the mode denote its degeneracy. The labelling of the representations at high-symmetry, non-zone-centre points is that of Zak (1969). The labelling of zone-centre representations is that of Mulliken (Mulliken 1933; Bradley and Cracknell 1972)

Wavevector	Rigid-unit mode
0,0,0 (Γ)	$A_2^{a} + E^{a} + B_1$
ξ,ξ,0 (ε)	${}^2\varepsilon_3$
½,½,0 (M)	${}^2M_2$

[a] A_2 and E are acoustic modes

spectra do not represent a true density of states. However, for RUMS, whose frequency is nearly independent of wave vector (e.g., see lattice dynamics calculations of Hua et al. 1989), it is a reasonable average. Figure 1 shows the low-frequency part of the spectrum, displaying a dramatic increase in the number of modes below ca. 40 cm^{-1} in the β-phase as compared to the α-phase, showing the origin of the additional disorder in the β-phase to be phonon-induced (Swainson and Dove 1993a).

Experimental

Infrared spectroscopy

The IR absorption experiments reported here used a Bruker 113 v Fourier transform IR spectrometer in the Department of Earth Sciences, University of Cambridge. Experiments were performed in both the mid-infrared (MIR), in the region of ca. 500–5000 cm^{-1}, and the far-infrared (FIR), the region of ca. 200–700 cm^{-1}. The sources of radiation for these two regions of the IR are, respectively, a graphite glowbar and mercury vapour lamp.

The furnace used in the experiments consists of a Pt-wound element encased in a water-cooled ceramic surround. A Pt–$Pt_{90}Rh_{10}$ thermocouple was used to record the internal temperature. The maximum operating temperature of the furnace was about 623 K. For the experiments performed below room temperature, a Leybold closed-cycle liquid-He cryostat was used in conjunction with a Leybold LTC 60 temperature controller, and the sample was kept under vacuum with the use of a rotary pump. Thermal stability was better than ± 1 K.

The spectra were fitted using Voigt functions to describe the line profiles. The peak positions, half widths and intensities reported here have maximum errors of the order of ± 0.2 cm^{-1}, ± 0.2 cm^{-1} and $\pm 5\%$, respectively.

Raman spectroscopy

The Raman experiments were performed using a Coderg T800 spectrometer at the Department of Physics, University of Edinburgh. The light source in this laboratory consisted of a Coherent Radiation Ar-laser Model 52, using a regulated DC ion laser power supply.

The furnace was a large copper block with four optical windows. The sample sat in the centre of the furnace in a vertical hole with a large copper plug on top. Four heating elements were placed into grooved slots in the copper. A Thor Model 3010II temperature controller was used in conjunction with a back-up Variac-controlled heater and a K-type thermocouple to measure furnace temperatures. The temperature variation was much less than 0.5 K.

The experiments were performed with 900 scattering geometry, and the laser was run at a nominal power supply of 400 mW under constant light conditions. The laser was tuned to the green Ar lasing line at 514.5 nm. The estimated error in frequency shift is ± 2 cm^{-1} across the whole range.

Samples

The samples used in the IR and Raman spectroscopy studies were prepared by devitrification of a silica glass supplied by Koch Light Laboratories Ltd., with a quoted purity of 99.9999% SiO_2. The cristobalite was synthesised by devitrifying the glass at 1773 K for 3 days and quenching the product in water. For the IR experiments the sample was ground using a mechanical mill for 15 min, and then mixed with a matrix, which was formed into a pellet. The matrix used in the MIR was KBr, and that in the FIR CsI. The proportions of 1:500 and 1:250 sample: matrix were used for the MIR and FIR experiments, respectively. The samples used in the Raman experiments were ground manually rather than mechanically and the sample holder was a silica glass capillary of diameter 0.5 mm.

Mode assignment

Group theory analysis of the normal modes in the α-phase of cristobalite

The decomposition of the zone centre irreducible representations in the α-phase is:

$$\Gamma_{\alpha}^{\text{total}} = 4A_1 + 5A_2 + 9E + 5B_1 + 4B_2 \ . \tag{2}$$

The acoustic modes transform as $A_2 + E$, so that the total representation containing only the optic modes is:

$$\Gamma_{\alpha}^{\text{optic}} = 4A_1 + 4A_2 + 8E + 5B_1 + 4B_2 \ . \tag{3}$$

The A_1, B_1 and B_2 modes are Raman-active only, the A_2 modes are IR-active only, and the E modes are both Raman- and IR-active. Thus, we expect 21 Raman-active modes and 12 IR-active modes, 8 of which are both Raman and IR-active. As noted by Etchepare et al. (1978) and Cherukuri et al. (1985) most of the E-symmetry bands are weak in the Raman spectra.

Relationship to the β-phase

The total decomposition of the zone centre representation of the β-phase is:

$$\Gamma_{\beta}^{\text{total}} = A_{2u} + E_u + 3T_{1u} + T_{2u} + T_{2g} \ . \tag{4}$$

The acoustic mode is of symmetry T_{1u} so that the total decomposition for the optic modes is:

$$\Gamma_{\beta}^{\text{optic}} = A_{2u} + E_u + 2T_{1u} + T_{2u} + T_{2g} \ . \tag{5}$$

Of these, T_{2g} is Raman-active and T_{1u} is IR-active, and because the cell is centrosymmetric, no modes are active in both spectra. There are therefore only one Raman-active fundamental and two infrared-active fundamentals in the spectra of β-cristobalite. Etchepare et al. (1978) give experimental data for the Raman-active modes, and we have measured IR spectra in this phase. A Raman mode was found at 777 cm^{-1} and IR modes were measured at 450 and 1087 cm^{-1}. Our calculations, performed using an ideal structure for the β-phase, indicate that there is a large TO/LO splitting of the T_{1u} modes, of the order of 100 and 180 cm^{-1}, respectively. This is larger than the splitting of the E and A_2 modes in the α-phase.

The total decomposition at the X-point in β-cristobalite was calculated using GROUP (Warren and Worlton 1974) and is given by:

$$X_{\beta}^{\text{total}} = 3X_1 + X_2 + 2X_3 + 3X_4 \ , \tag{6}$$

where we use the labelling of Zak (1969). These modes become zone centre modes in the α-phase.

The compatibility between the Γ- and X-point modes in the β-phase and the Γ-point modes in the α-phase is given in Table 3.

Experimental data

A number of tabulations of the peaks in the Raman and IR spectra of the α-phase of cristobalite have been published (Bates 1972; Etchepare et al. 1978; Cherukuri et al. 1985).We present a tabulation of the calculated mode frequencies of the various groups in Table 4. The tabulation of the observed mode frequencies in Tables 4 and 5 excludes all modes for which there does not appear to be adequate experimental evidence. Bates (1972) has observed 13 Raman-active modes at 77 K. Thus, 8 Raman-active modes have

Table 3 Compatibility diagram showing correlation between the Γ- and *X*-point optic modes of the *β*-phase and those of the Γ-point of the α-phase

β-phase		α-phase			
A_{2u}	→				B_2
E_u	→	A_1		+ B_2	
$2T_{1u}$	→		$2A_2$ + $2E$		
T_{2u}	→		E + B_1		
T_{2g}	→		E + B_1		
$3X_1$	→		$3E$		
X_2	→		E		
$2X_3$	→		$2A_2$		+ $2B_2$
$3X_4$	→	$3A_1$	+ $3B_1$		
Total		$4A_1$ + $4A_2$ + 8E + $5B_1$ + $4B_2$			

not been seen. We exclude the reported Raman mode at 447 cm^{-1} (Cherukuri et al. 1985) as this is difficult to determine from examining their data.

We measured 11 IR modes at 31 K, with one mode absent. Additional modes have been extracted from reflectance spectra of other workers, but these spectra are difficult to interpret and we believe that some of the modes are spurious. For example, the reported mode at 1040 cm^{-1} (Cherukuri et al. 1985) is difficult to substantiate.

Assignment of observed modes in the α-phase of cristobalite

There have been three previous but conflicting mode assignments of the IR and Raman spectra of α-cristobalite. We will attempt to use additional data and calculations to determine a new assignment. Unfortunately, the fact that three irreducible representations are Raman-active means that it is difficult to assign the modes using

Table 4 Results of the normal-mode analysis at the zone centre (frequencies in cm^{-1}) and mode assignments for the α-phase of cristobalite. *Sanders* and *S* denote our calculations using the model of Sanders et al. (1984); *Cherukuri* and *C* the results from Cherukuri et al. (1985); *Etchepare* those of Etchepare et al. (1978). The results from each potential are ordered in terms of calculated frequency. The *seventh column* gives the corresponding irreducible representation in the *β*-phase, as referenced to the Sanders et al. (1984) potential. The *last two columns* contain the experimental values. They are paired with their assigned modes in the Sanders column. The Raman data of the lowest B_1 are from the room-temperature measurements by Sigaev et al. (1999), and the rest are from the 77 K data of Bates (1972). The infrared data are from our measurements at 31 K. Unobserved modes are indicated by "—". Uncertainties in the assignments are indicated in two ways: a frequency that may be assigned to more than one possible symmetry is given in *brackets*. One case where there are there are two candidate modes for two symmetries is indicated by giving both frequency values separated by a "/"

	Etchepare		Cherukuri		Sanders		*β*	IR	Raman	
Anti-symmetric Si–O–Si stretch	B_1	1189	B_2	1195	A_2	1121	T_{1u}	1144		Γ = $A_1 + A_2$ $+B_1 + B_2$ $+E$
	E	1137	E	1164	E	1077	X_1/X_2	1196	1193	
	A_2	1089	E	1085	B_2	944	A_{2u}		1188	
	B_1	1084	A_1	1066	E	927	T_{1u}	1100	–	
	E	1082	B_1	1013	B_1	925	X_4		1076/ 1086	
	A_1	1081	A_2	1008	A_1	924	X_4		1076/ 1086	
Symmetric Si–O–Si stretch	B_2	770	E	773	E	822	T_{2g}	797	796	Γ = A_2 + B_1 + B_2 + E
	A_2	767	B_2	756	A_2	821	X_3	–		
	B_1	767	B_1	756	B_2	815	X_3		–	
	E	760	A_2	709	B_1	811	T_{2g}		785	
	E	634	E	631	E	622	X_1/X_2	625	–	
Lattice and O–Si–O bending modes: not RUMs in either phase	E	489	A_2	495	A_2	534	T_{1u}	495		C and S agree on order of A_1 + A_2 + B_2 + E
	A_2	488	E	458	E	441	T_{1u}	480	–	
	A_1	430	B_2	446	B_2	411	E_u		(426)	
	B_1	414	A_1	429	A_1	384	E_u		(426)	
	A_1	376	E	420	B_1	365	X_4		(368)	A_1 + B_1 + E: No agreement
	E	368	A_1	364	E	364	X_1/X_2	380	380	
	B_1	366	B_1	342	A_1	340	X_4		(368)	
	A_2	303	A_2	314	A_2	285	X_3	300		All agree on order of A_1 + A_2 + $2B_1$ + B_2 + E
	B_2	285	B_2	285	B_2	271	X_3		286	
	E	272	E	267	E	255	X_1/X_2	276	275	
β-RUMs	A_1	231	A_1	236	A_1	196	X_4		233	
	E	129	E	145	E	143	T_{2u}	147	–	
	B_1	94	B_1	140	B_1	111	X_4		121	
	B_1	75	B_1	94	B_1	32	T_{2u}		50	

only the selection rules with data from powdered samples. Moreover, as we note above, not all the modes that are active in either Raman or IR spectra are observable.

The earliest assignment was attempted by Bates (1972), who performed an IR and Raman study of cristobalite in both the β-phase and in the α-phase. The assignment was based upon analogy to the spectra in quartz. The assumption made was that modes that were of similar frequency in the two spectra must be due to the same fundamental vibrational motion. Bates used a correlation method to correlate the point group of α-quartz, D_3, to that of α-cristobalite, D_4, via the common C_2 silicon site symmetry present in both space groups. Unfortunately, the silicon site is of such a low symmetry (possessing only two representations) that most unambiguous correlation information is lost. Criticisms of the method of Bates (1972) have also been made by Etchepare et al. (1978), although both arrived at very similar assignments (Table 5).

Etchepare et al. (1978) and Cherukuri et al. (1985) have given assignments that were obtained on a more rigorous basis, using normal mode calculations with force constant models calculated for quartz, and comparing the calculated frequency values with the observed Raman and IR spectra. A further check was incorporated in the study of Cherukuri et al. (1985) by comparing calculated and observed mode frequency shifts in pure ^{28}Si- and ^{29}Si-cristobalite.

We have calculated mode frequencies using a model developed for SiO_2 by Sanders et al. (1984). This is an empirical potential that consists of a Born model for short-range interactions with some dispersive interactions, formal charges, a shell model for the oxygen atoms and a harmonic potential to describe flexing of the O–Si–O angles. Our calculations are compared with those of Cherukuri et al. (1985) and Etchepare et al. (1978) in Table 4, where the mode assignments from each potential is listed in order of their calculated frequency. The modes are also separated into ''bands'' of frequency-separated groups with similar broad characteristics (e.g., ''anti-symmetric T–O–T stretch'').

The compatibility between individual modes in the β- and α-phases was determined in the following manner. The decomposition of the modes at the Γ-points (Eqs. 2–5) of both phases was determined using the correlation method (Fateley et al. 1972), and that of the X-point of the β-phase was determined using the symmetry analysis program GROUP (Warren and Worlton 1974). This program outputs a character table with numbered representations. It was possible to correlate these to specific symmetries using published character tables and other knowledge such as the symmetry of the acoustic modes and the total decompositions (Eqs. 2–6) at these points in the Brillouin zone.

With the method outlined above it was then possible to assign modes in both the α- and β-phases, using the known compatibility relationships of Table 3. The lattice dynamic calculations were repeated for α-cristobalite, artificially changing the value of the order parameter, Q (as defined by Schmahl et al. 1992), continuously towards a value of zero, taking into account the large change in lattice parameters through the transition. This artificially made the transition continuous and, by tracking the change in calculated frequency of each assigned Γ-point mode in the α-phase as it changed into the β-phase, it was possible to determine the individual compatibility of each Γ-point mode in the α-phase with Γ- and X-point modes in the β-phase. This is necessary since, e.g., a B_1 mode in α-cristobalite can transform to T_{2u}, T_{2g} or X_4. In most cases the assignments of the IR- and Raman-active modes in each phase agree with those of Cherukuri et al. (1985) and Etchepare et al. (1978).

The natural division of the modes in Table 4 in silica into frequency-separated ''bands'' with broad similarities, e.g., symmetric T–O–T stretching, aids comparison. One can see that within ''bands'', e.g. the antisymmetric and symmetric T–O–T stretches, the global compatibility relationships in Table 3 appear to have translated into reasonable individual compatibilities: all anti-symmetric T–O–T stretch modes in the α-phase transform to anti-symmetric T–O–T stretch modes in the β-phase without having to resort to unreasonable hybridization across bands.

The agreement between the three potentials is generally reasonable, although some large disagreements are present, in particular in the internal T–O–T stretch modes (Table 4). One can see that, in general, although the specific calculated frequencies differ, the external modes (below ca. 650 cm^{-1}), when placed in order of frequency, agree very well, particularly between our calculations (''Sanders'' in Table 4) and those of Cherukuri et al. (1985). There are some uncertainties that cannot be resolved:

- The ambiguities of the Raman modes at 368 cm^{-1} arise from the fact that the two candidate assignments, A_1 and B_1, are correlated to the same mode, X_4, in the β-phase. This mode is

Table 5 Comparison of various assignments of infrared and Raman-active modes in α-cristobalite. Here the observations (from the same sources as Table 4) are ordered in terms of observed frequency

Observations		Assignments			
IR	Raman	Sanders	Cherukuri	Etchepare	Bates
1196	1193	E	(B_2) or E		E_1 or B_1 or B_2
	1188	B_2			
1144		A_2			
1100		E	E		E_1
	1086	B_1 or A_1			
	1076	A_1 or B_1	A_1	A_1	A_1
798	796	E	E	E_t	E_1
	785	B_1	B_1 or B_2	E_1	E_t
625		E	E	A_2	A_2
495		A_2	A_2	A_2	A_2
480	485?	E	E	$E_t + E_1$	$E_t + E_1$
	426	A_1 or B_2	A_1	A_1	A_1
380	380	E	E	E_t	E_t
	368	A_1 or B_1	A_1 or B_1	B_1	B_1
300		A_2	A_2		A_2
	286	B_2	B_2	$E_t + E_1$	$E_t + E_1$
276	275	E	E	B_1 or B_2	B_1 or B_2
	233	A_1	A_1	A_1	A_1
147		E	E	E	$E_t + E_1$
	121	B_1	B_1	E	$E_t + E_1$
	50	B_1	B_1		

double-degenerate in the β-phase, yet only one is seen in the spectra of the α-phase.
- The ambiguities of the Raman modes at 426 cm^{-1} also arise from a splitting of a two-dimensional mode, E_u, in the β-phase into two one-dimensional modes, A_1 and B_2, of which one is apparently silent.
- The two modes at 1076 and 1086 cm^{-1} both have the same double-degenerate parent mode in the β-phase, X_4, and it is not possible to say which of these is A_1 and B_1 in the α-phase.

The other assignments are, we believe, unambiguous.

Results

Infrared data

The temperature dependence of the FIR (in the range 200–650 cm^{-1}) and MIR spectra (over the range 550–900 cm^{-1}) are shown in Figs. 2 and 3, respectively. The FIR spectra at low temperatures contain three sharp peaks corresponding to the 300 cm^{-1} ($A_2 \leftrightarrow X_3$), 380 cm^{-1} ($E \leftrightarrow X_1/X_2$) and 625 cm^{-1} ($E \leftrightarrow X_1/X_2$) modes, and one large structured peak at low temperatures which contains the 480 cm^{-1} ($E \leftrightarrow T_{1u}$) and 495 cm^{-1} ($A_2 \leftrightarrow T_{1u}$) modes. At high temperatures the only remaining peak is the T_{1u} mode at 500 cm^{-1}. Figure 3 shows two sharp peaks in the range displayed at 625 cm^{-1} (E) and 797 cm^{-1} (E). Another sharp peak occurs at higher energies at 1196 cm^{-1} (E) modes, and one structured peak containing the 1100 cm^{-1} ($E \leftrightarrow T_{1u}$) and 1144 cm^{-1} ($A_2 \leftrightarrow T_{1u}$) modes. We have not shown these internal modes in Fig. 3, but we refer the interested reader to the diffuse reflectance and emission spectra of Finnie et al. (1994). At high temperatures the only remaining peaks are the broad peaks at 797 and 1100 cm^{-1}.

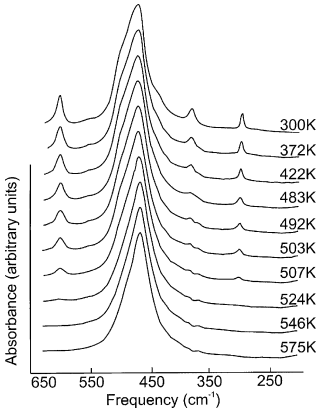

Fig. 2 FIR spectra of cristobalite in the range 200–650 cm^{-1} through the transition. The 625 cm^{-1} mode is visible due to the overlap with the MIR source. The 300 cm^{-1} mode, of A_2 symmetry, disappears above T_{tr}

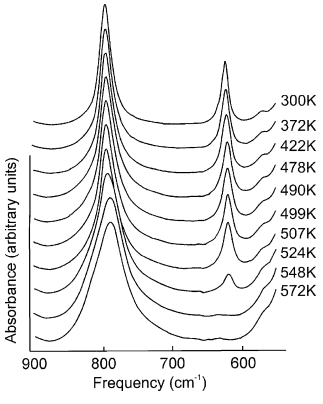

Fig. 3 MIR spectra of cristobalite as a function of temperature in the range of 550–900 cm^{-1}. There is considerable broadening of the mode near 797 cm^{-1} above T_{tr}

Most of the peaks show no unusual behaviour. Figure 4 shows the frequency and FWHM of the modes near 790 cm^{-1} as a function of temperature, whose behaviour is quite complicated. Figure 5 shows the behaviour of two modes which transform to zone-boundary modes in the β-phase. Near T_{tr}, both show anomalies in behaviour. Both show a gradual rather than a sudden, decline in intensity, In addition, other anomalies are present. In the case of the 300 cm^{-1} ($A_2 \leftrightarrow X_3$) mode (Fig. 5a) it appears most pronounced in the behaviour of the frequency, whereas in the case of the 625 cm^{-1} ($E \leftrightarrow X_1/X_2$) it is the FWHM (Fig. 5b).

Raman data

Prior to heating, several scans were taken at room temperature, as the signal was much stronger than when the sample was in the furnace. This allowed the observation of some of the weaker modes. We observed modes at 114 cm^{-1} ($B_1 \leftrightarrow X_4$), 231 cm^{-1} ($A_1 \leftrightarrow X_4$), 275 cm^{-1} ($E \leftrightarrow X_1/X_2$), 286 cm^{-1} ($B_2 \leftrightarrow X_3$), 418 cm^{-1} ($A_1/B_2 \leftrightarrow E_u$), 785 cm^{-1} ($B_1 \leftrightarrow T_{2g}$), 1083 cm^{-1} ($B_1 \leftrightarrow X_4$) (very broad, see below) and 1188 cm^{-1} ($A_1 \leftrightarrow X_4$) cm^{-1} at room temperature, out of the furnace. All these modes are clearly shown in the spectra of Bates (1972). We also observed a very low-frequency mode on the Rayleigh wing, which has been reported by Sigaev et al.

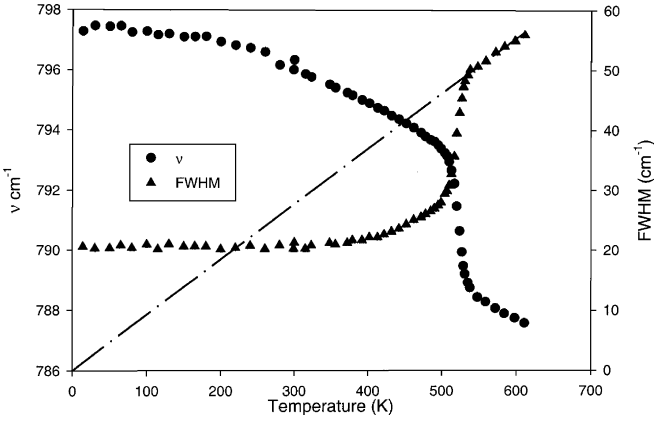

Fig. 4 Temperature dependence of the frequency and FWHM of the IR-active modes in the vicinity of 790 cm^{-1}

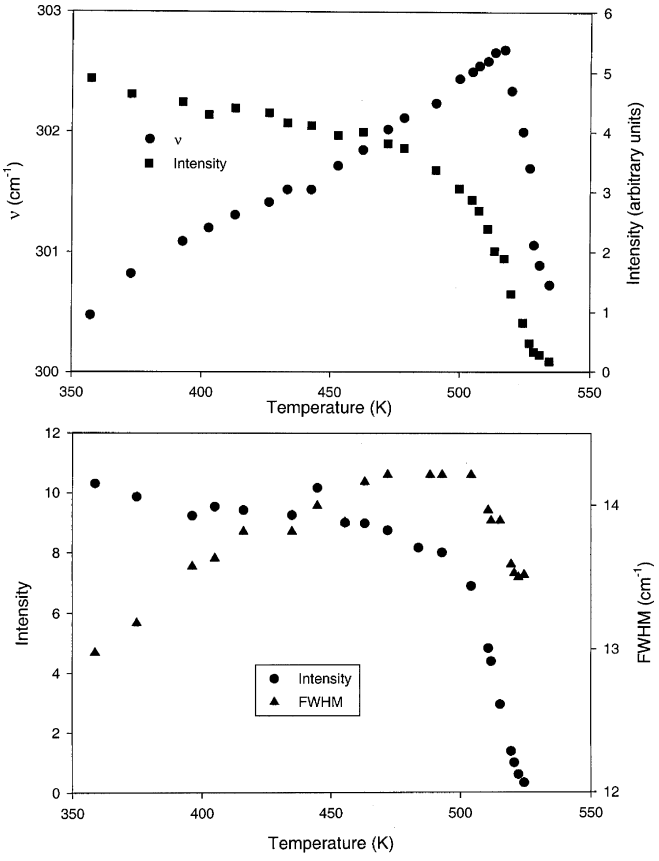

Fig. 5 **a** Temperature dependence of the frequency and intensity of the 300 cm^{-1} $A_2 \leftrightarrow X_3$ mode. **b** Temperature dependence of the integrated intensities and FWHM of the 625 cm^{-1} $E \leftrightarrow X_1/X_2$ mode

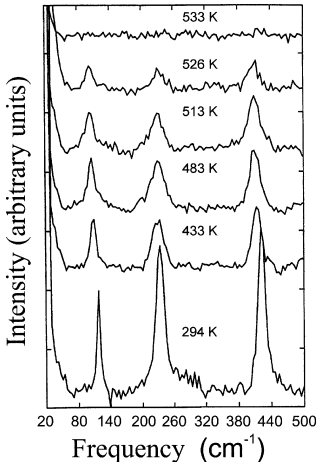

Fig. 6 Raman spectra of cristobalite as a function of temperature in the region of 20–520 cm^{-1}

(1999) at 50 cm^{-1}. The data of Bates (1972) suggest that the two high-frequency modes are both doublets – see Table 4.

For the heating runs the scanning region was confined to 20–520 cm^{-1}, as only the 114 cm^{-1} ($B_1 \leftrightarrow X_4$), 231 cm^{-1} ($A_1 \leftrightarrow X_4$) and 418 cm^{-1} ($A_1/B_2 \leftrightarrow E_u$) modes

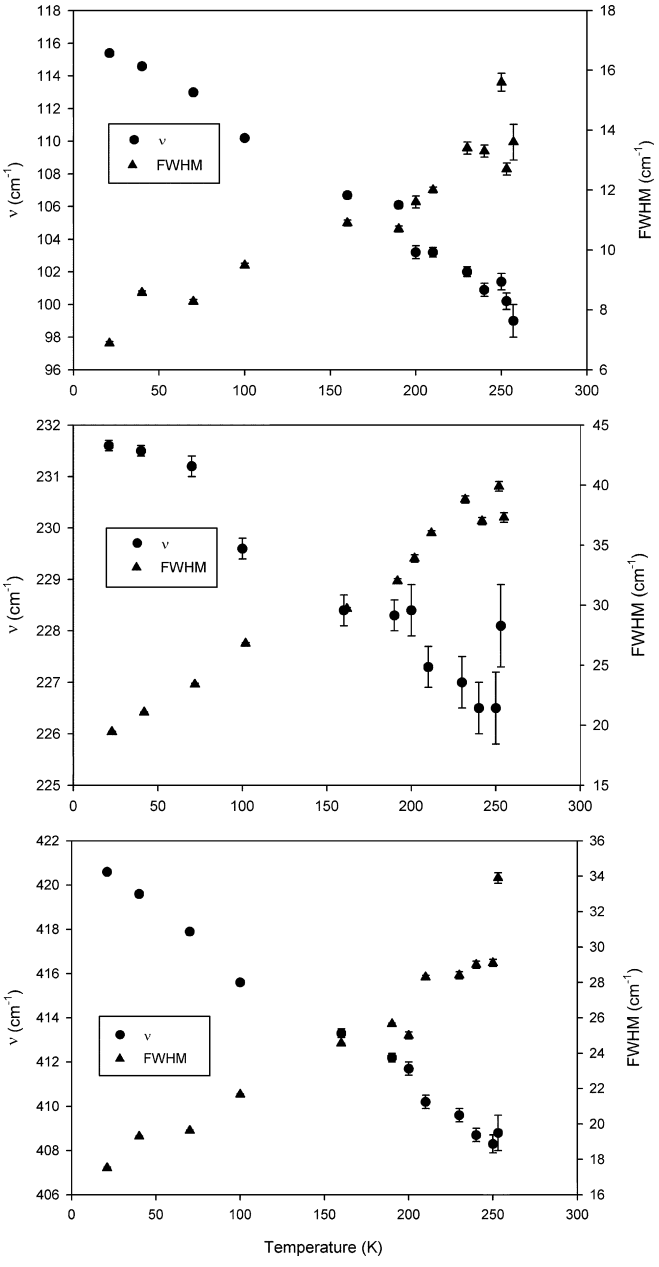

Fig. 7 Temperature dependence of the frequencies and FWHM of the Raman-active 114 cm^{-1} ($B_1 \leftrightarrow X_4$), 231 cm^{-1} ($A_1 \leftrightarrow X_4$) and 418 cm^{-1} ($A_1/B_2 \leftrightarrow E_u$) modes

were sufficiently strong that they could be followed when the sample was in the furnace. The spectra obtained are displayed as a function of temperature in Fig. 6, where all three modes disappear in the β-phase. Because of problems with fluorescence, the background of the spectra varied greatly, so that quantitative comparison of the mode intensities was not attempted.

The temperature dependence of the frequencies and FWHM of the 114 cm^{-1} ($B_1 \leftrightarrow X_4$), 231 cm^{-1} ($A_1 \leftrightarrow X_4$) and 418 cm^{-1} ($A_1/B_2 \leftrightarrow E_u$) modes are shown in Fig. 7. All three modes soften as the framework becomes less distorted on heating towards T_{tr}. Palmer et al. (1994) observed that these three modes increase in

frequency as pressure is applied and the framework becomes more distorted. The largest change in frequency is for the 114 cm^{-1} ($B_1 \leftrightarrow X_4$) mode.

Discussion

Comparison of the spectra of the α- and β- phases

The interpretation of the temperature dependence of the IR and Raman spectra needs to be approached with some care. Taking our data and the Raman data of Bates (1972), we find that the modes at 121 cm^{-1} ($B_1 \leftrightarrow X_4$), 233 cm^{-1} ($A_1 \leftrightarrow X_4$), 275 cm^{-1} ($E \leftrightarrow X_1/X_2$), 286 cm^{-1} ($B_2 \leftrightarrow X_3$), 300 cm^{-1} ($A_2 \leftrightarrow X_3$), 380 cm^{-1} ($E \leftrightarrow X_1/X_2$), 426 cm^{-1} ($A_1/B_2 \leftrightarrow E_u$), 625 cm^{-1} ($E \leftrightarrow X_1/X_2$), 1188 cm^{-1} ($B_2 \leftrightarrow A_{2u}$) and 1196 cm^{-1} ($E \leftrightarrow X_1/X_2$) vanish completely in the Raman and IR spectra on heating into the β-phase. These modes are all expected to vanish due to two reasons. First, some of these modes transform to a Γ-point representation that is inactive in the β-phase, e.g., the 1188 cm^{-1} mode changes from the Raman-active B_2 in the α-phase to the silent representation A_{2u} in the β-phase. Second, half of the zone centre modes in the α-phase will become X-zone boundary modes in the β-phase, e.g., the mode at 625 cm^{-1} changes from E symmetry in the α-phase to X_1/X_2 in the β-phase.

The modes in the α-phase at 785 cm^{-1} (B_1) and 797 cm^{-1} (E) remain in the Raman spectra of the β-phase as they combine to form the Raman-active T_{2g} mode, reported at 777 cm^{-1} by Bates (1972).

The pairs of modes in the IR spectra of the α-phase at 480 cm^{-1} (E) and 495 cm^{-1} (A_2), and at 1100 cm^{-1} (E) and 1144 cm^{-1} (A_2), combine to form the two IR-active T_{1u} modes in the β-phase. However, the frequencies of the combining pairs remain different due to LO/TO splitting. The 1100 cm^{-1} (E) mode becomes the transverse component of the T_{1u} mode in the β-phase, and is expected to remain IR-active in this phase as observed. The 1144 cm^{-1} (A_2) mode, which appears as a shoulder on the peak at 1100 cm^{-1}, becomes the corresponding longitudinal component of the T_{1u} mode in the β-phase. In absorption/transmission experiments the LO (higher frequency) component ought to be invisible, but can often be seen as a result of reflectance from some of the small grains in the sample.

Temperature dependence of modes

Soft modes

The transition pathway described below proposes that $X_4 \Rightarrow A_1 + B_1$, so the soft modes should be observable in the Raman spectra of the α-phase. One of the low-frequency B_1 modes must be one component of the soft mode. From our mode assignments, we find that the soft modes in the α-phase are the 231 cm^{-1} ($A_1 \leftrightarrow X_4$) and 121 cm^{-1} ($B_1 \leftrightarrow X_4$) modes – the assignment of the 231 cm^{-1} ($A_1 \leftrightarrow X_4$) soft mode agrees with the eigenvector calculations of Etchepare et al. (1978). Neither the 231 cm^{-1} ($A_1 \leftrightarrow X_4$) nor the 121 cm^{-1} ($B_1 \leftrightarrow X_4$) modes are RUMs in the α-phase. These frequencies may at first sight appear to be large for soft modes, but it is worth noting that in quartz the frequency of the soft mode is about 207 cm^{-1}, and even in this much less discontinuous system the mode does not soften completely (Shapiro et al. 1967). From Table 4 we see that there is another B_1 mode at a calculated frequency of 32 cm^{-1}. This has been observed recently (Sigaev et al. 1999) at 50 cm^{-1}. We believe that this mode is the B_1 RUM (Table 2), which becomes degenerate with the 147 cm^{-1} E mode (Table 3) to become the T_{2u} optic RUM in the β-phase (Table 1).

Hard modes

Mode coupling

The frequencies of the hard phonon modes can vary with order parameter, Q, in two ways: a singlet mode (and a mode which remains double-degenerate in both phases) will change frequency as $\Delta\omega \propto Q^2$ to lowest order, and a degenerate mode, which loses its degeneracy, as $\delta\omega \propto aQ + bQ^2$, where a can be zero or non-zero depending on symmetry constraints. Each mode has its own unique coupling constants, so that some modes may show stronger temperature dependence than others. Since the temperature dependence of Q is already known from neutron powder diffraction data (Schmahl et al. 1992), we have not attempted to use the spectroscopy data to determine the temperature dependence of Q again. Also, there are not enough data in the high-temperature phase to enable us to determine frequency changes of the required accuracy, since most of the phonon peaks vanish above T_{tr}.

The IR-active 625 cm^{-1} ($E \leftrightarrow X_1/X_2$) mode has a relatively large change in frequency with temperature (Fig. 5b). This mode remains double-degenerate in both phases and its behaviour is expected to follow the same behaviour as for the singlet modes described above (Dove 1993; Petzelt and Dvorak 1976a). Indeed, the temperature dependence of the frequency is consistent with a low-order expansion in Q. The same is also true of the Raman-active 426 cm^{-1} ($A_1/B_2 \leftrightarrow E_u$) mode, which follows the expansion for a mode that splits in the low-symmetry phase.

The behaviour of the IR-active 300 cm^{-1} ($A_2 \leftrightarrow X_3$) mode is more complicated. Here we discuss the region away from the "transition region" (500–550 K), which is discussed in more detail in the next section. This mode also has a relatively large change in frequency on cooling. We associate this mode in the α-phase as the higher-frequency component of a split mode (Table 4), the other component being the weak Raman-active 286 cm^{-1} ($B_2 \leftrightarrow X_3$) mode observed by Bates (1972). It may be

expected that this mode would increase in frequency on cooling, whereas from Fig. 5a we can see that it actually decreases in frequency on cooling, below ca. 500 K. For a mode which loses its degeneracy (in this case the two-dimensional X_3 mode), a form such as $\delta\omega = \omega_{A_2} - \omega_{B_2} = aQ + bQ^2$, with $a > 0$ and $b < 0$, is expected (Petzelt and Dvorak 1976a,b, Dove 1993). For various values of a, b the following special cases may be observed:

- For small Q the B_2 mode will have the larger frequency, and the difference in frequencies will increase on cooling.
- However, when $Q = -a/2b$ the frequency splitting is a maximum, and as Q increases on further cooling the splitting will decrease again.
- If we could cool to $Q = -a/b$ the two frequencies would be the same, and at larger values of Q the A_2 mode would have the larger frequency.

Our data are consistent with this picture of splitting, if over the temperature range from 0 K to T_{tr}, Q exists between $-a/b$ and $-a/2b$, so that the A_2 mode has a higher frequency than the B_2 mode, but on cooling (increasing Q) the two frequencies become closer, leading to a decrease in the frequency of the A_2 mode. This behaviour has been previously observed in the phase transition in the molecular crystal *sym*-triazine (Rae 1982; Ewen and Dove 1983). Further, detailed measurements of the temperature dependence of the Raman spectrum of the weak B_2 mode would confirm or refute this explanation.

The effect of coexistence on mode intensity, frequency and linewidth

The cristobalite transition is highly first-order: a typical Landau picture of a first-order transition is shown in Fig. 8, where $G(Q)$ represents the Landau free energy as a function of order parameter, Q. In cristobalite, the first-order step ΔQ at T_{tr} is about 60% of the saturated value of Q at 0 K (Schmahl et al. 1992). One may therefore expect large jumps in the behaviour of the inelastic spectra of cristobalite through the transition region. However, it is apparent that many of the features seen in the IR and Raman spectra are much smoother than would be expected from Fig. 8a. These effects are not primarily caused by temperature gradients, but by coexistence. As one is measuring the average across many grains, the inelastic measurements ref lect an average measure of structural state of the whole sample. Coexistence in the transition region therefore affects what is measured dramatically.

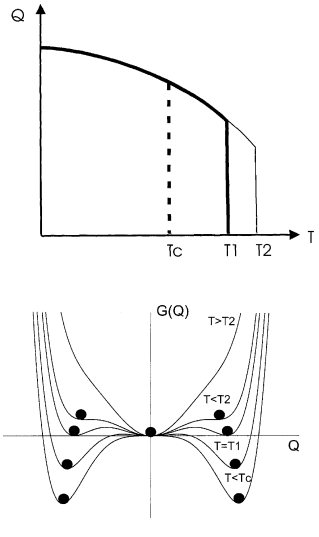

Fig. 8 **a** Diagram of order parameter, Q, versus temperature, T, of a first-order transition and **b** of Landau free energy, G, versus order parameter, Q, as a function of temperature

Coexistence of α- and β-cristobalite is a natural outcome of the first-order nature of the transition. Coexistence has been previously observed in neutron and X-ray powder scattering (Schmahl et al. 1992), DSC (Schmahl 1993) and NMR (Spearing et al. 1992; Philips et al. 1993). One form of coexistence takes place within a single grain: distinct regions of α-phase coexist with regions of β-phase. Krisement and Trömel (1959a,b) estimated the transition time for a single grain to be less than 0.1 s from optical observations. This is similar to the situation in certain athermal martensites, where rapid transition times make direct observation of coexistence impossible. In such cases the only evidence for coexistence of α- and β-forms within a single grain is the retention of trapped β-phase, which has been reported in cristobalite (Nord 1994). However, it has also been observed that different grains of cristobalite have different T_{tr}s (Krisement and Trömel 1959a,b) so that macroscopic coexistence also occurs between grains. This form of coexistence has the greatest temperature range. The different T_{tr}s may be due to different residual stresses/defects in the grains requiring a different driving force for transition which can renormalize T_c for each grain. A variety of T_{tr}s have also been reported in cristobalite as a function of temperature of formation, which explains the very different values of T_{tr} reported through the literature (for review, see, e.g., Sosman 1965).

The phenomenon of coexistence can be described in the Landau formalism by Fig. 8a and b. On heating, the system reaches the state where α-($Q \neq 0$) and β-cristobalite ($Q = 0$) are in equilibrium at T_1 (Fig. 8b). At this point some of the grains may transform, but there is an activation energy to overcome. The $Q \neq 0$ minimum persists as a local minimum up to T_2, at which point it disappears, and all the grains have transformed to β-cristobalite. In the region (T_1,T_2) a proportion of the cristobalite grains can remain metastably in the α-form, giving rise to a variety of observed T_{tr}s, even if all the grains had the same potential and T_c. If, as suggested above, there is, in addition, a distribution of T_cs across the grains, the coexistence region is further smeared out over a wider temperature interval.

Intensity

Figure 5 appears to be consistent with coexistence in the range of ca. 500–550 K. For $T < 500$ K, well below the transition region, the intensities of such modes vary due to changes associated with the transition in the structure factor of the modes. While there is no sudden decrease to zero intensity there is a smooth change in slope above 500 K, which is indicative of coexistence, particularly in the 300, 625 and 797 cm^{-1} modes. As the proportion of cristobalite existing in either α- or β-forms will vary smoothly with temperature, a smooth decrease in the intensity of these modes is observed.

Frequency

Coexistence is correlated with a continuous change in mode frequency for these modes through this temperature range (Fig. 5). For grains sharing an identical potential (and therefore T_c) those grains that remain untransformed above T_1 continue to change state (Q), as shown by Fig. 8, at which point they jump to the β-phase and cease to contribute to the signal. Again, this can be further affected by the persistence of other grains with slightly different potentials (higher T_cs).

Linewidth

Above about 480 K the linewidth of the IR-active 625 cm^{-1} ($E \leftrightarrow X_1/X_2$) mode apparently begins to decrease on heating. This is opposite to normal behaviour, as anharmonicity generally increases with temperature. This does not appear to be an artifact induced by fitting to a mode of declining intensity, as at ca. 500 K, where this effect begins, the intensity has dropped to only 80% of that seen at room temperature (Fig. 5b). A similar, although less pronounced effect, was observed in the 300 cm^{-1} ($A_2 \leftrightarrow X_3$) mode. The effect is clearly associated with the coexistence region. One possibility is if different grains have different T_cs, and therefore different non-zero values of Q at the same temperature. As temperature increases and progressively more grains transform to the β-phase, becoming silent in the IR, the distribution of different Q-states at any temperature sharpens, resulting in narrower absorption bands. Such an explanation would be consistent with a continuous narrowing of the modes in the transition region until they disappear.

Anomalies in the β-phase

We noted above that there are peaks in both the Raman and IR spectra of the β-phase that are expected to be absent by symmetry: the mode at 1076 cm^{-1} in the Raman spectra and the mode near 789 cm^{-1} in the IR spectra. The width of the 789 cm^{-1} IR mode in the β-phase, shown in Fig. 4, is of the order of 60 cm^{-1} at 600 K.

It is tempting to suggest that the mode near 789 cm^{-1} in the β-phase is a "forbidden mode" directly related to the 797 cm^{-1} $E \leftrightarrow T_{2g}$ fundamental in the α-phase, perhaps suggesting that β-cristobalite is made up of α-domains. However, as discussed earlier, in the case of quartz such arguments for forbidden modes were made early on and shown to be false. Instead, it is likely that it is not a fundamental. The strongest argument against a forbidden mode is that if it were a persistent E-mode from domains of α-cristobalite then the modes seen in the β-phase in both the Raman and IR would be expected to have the same frequency. This is indeed the case in the α-phase (Table 4 in Bates 1972): Bates reports the Raman frequency at 77 K as 796 $\pm$ 1 cm^{-1} and we find it in the IR at 797 cm^{-1} at this temperature. However, Bates reports a mode in Raman spectra of the β-phase at 777 cm^{-1} at 551 K, whereas we see that in the IR it is closer to 788 cm^{-1} at this temperature.

Finnie et al. (1994) have suggested it is a two-phonon combination band involving the coupling of the 777 cm^{-1} Raman-active T_{2g} mode with the lowest frequency T_{2u} mode. This is the optic zone-centre RUM in the β-phase. This appears to be a likely explanation as:

- The symmetry is correct. The two-phonon combination band would have the symmetry of $T_{2g} \otimes T_{2u} = A_{2u} + E_u + T_{1u} + T_{2u}$. Since this contains T_{1u} it may be IR-active (Alpert et al. 1970). However, as it does not contain T_{2g}, this should not be visible in the Raman spectra.
- The frequency is approximately correct. The frequency of the T_{2u} RUM in the β-phase is not known. However, in the α-phase it splits into a non-RUM E-mode and the RUM B_1 mode, reported at 50 cm^{-1} at room temperature (Sigaev et al. 1999). In general, the frequency of a combination band is slightly lower than the sum of the two contributing modes (Alpert et al. 1970). We can therefore put a lower bound on the frequency of the T_{2u} RUM at 551 K of ≥ 11 cm^{-1}.

In summary, in the IR, the "mode" in the 797 cm^{-1} region is a single-phonon E-mode in α-cristobalite, which appears to be "replaced" by a two-phonon process, $T_{2g} \otimes T_{2u}$, above T_{tr}. In the Raman, the mode seen near this region is the $E \leftrightarrow T_{2g}$ one-phonon fundamental. This $E \leftrightarrow T_{2g}$ Raman mode at 777 cm^{-1} and the T_{2u} RUM are the "parent" excitations of the combination band seen in the IR spectra of the β-phase.

The two-phonon 797 cm^{-1} mode is very broad (Fig. 6). It is quite likely that the large widths arise simply from strong anharmonic interactions, consistent with the width varying linearly with temperature.

The 1078 cm^{-1} mode observed in the Raman spectra of the β-phase may also be due to a higher-order process, as there are no T_{2g} modes in the antisymmetric stretch region (Table 4). It is also fairly broad, as was demonstrated by Bates (1972).

There is also an extremely broad feature at 267–292 cm^{-1} reported by Bates (1972) in the Raman spectra of the β-phase. This was not reported by Etchepare et al. (1978), and not observed by us, so we offer no explanation.

Anomalies in the α-phase

There is also at least one possible two-phonon process in the IR spectra of α-cristobalite. The broad band near 500 cm^{-1} (Fig. 2) contains the A_2- and E-modes, but there is a distinct shoulder at room temperature on the low side (ca. 440 cm^{-1}) that broadens and disappears on heating. This is in the correct frequency range for a combination of the 147 cm^{-1} E-mode and the A_2 mode at 303 cm^{-1}. The direct product of these modes is also E. Since this is both IR- and Raman-active, one might expect it in both spectra. Unfortunately, E-modes are weak in the Raman spectra (Etchepare et al. (1985)) and this lies on top of the suggested position for a B_2 mode by Cherukuri et al. (1985), itself in the tail of a third mode, the 426 cm^{-1} ($A_1/B_2 \leftrightarrow E_u$) Raman mode. It is therefore very difficult to test unambiguously.

When phonon linewidths arise solely from lowest-order anharmonic interactions, they should show a linear temperature dependence that extrapolates to zero width at 0 K (neglecting quantum effects). In the Raman spectra, the linewidths are consistent with such an extrapolation, within error. The saturation at a width of 20 cm^{-1} seen in the 797 cm^{-1} ($E \leftrightarrow T_{2g}$) mode throughout the α-phase is extremely unusual. Two possible explanations come to mind:

- It is due to the grain size of the sample. That such broadening is observed in only one mode is evidence against this. Measurements were performed on samples ground for 5, 10 and 20 min. No significant effect was seen in the FWHM,
- This mode may consist of two overlapping modes appearing as one at all temperatures in the α-phase. Table 4 shows an IR-active A_2-mode at a calculated frequency of 822 cm^{-1} and IR-active E-mode at 821 cm^{-1}. The calculated data of Cherukuri et al. (1985) show a much greater splitting of about 60 cm^{-1}. This seems an unlikely explanation, but we are unable to offer any other at this time.

Conclusions

We have presented IR and Raman spectra of α- and β-cristobalite as a function of temperature through the phase transition in much finer temperature intervals than has been published before. The compatibility between X- and Γ-points of the β-phase and the Γ-phase of the α-phase are used to understand the mode assignments in the two phases. The IR and Raman spectra of the β-phase are sufficiently different from the α-phase for it to be difficult to invoke well-defined α-domains as a model for β-cristobalite.

The region near 777–797 cm^{-1} in the IR and Raman spectra of α- and β-cristobalite is complicated. The IR "band" in this region is a one-phonon mode in the α-phase which is replaced by a two-phonon process in the β-phase, as first suggested by Finnie et al. (1994). The mode that appears in the Raman spectra of the β-phase at ca. 777 cm^{-1} is one parent of this two-phonon process in the IR.

The rather smooth reduction in intensity, narrowing of linewidths and smooth variation in intensity of some of the IR-active modes that disappear in the β-phase seem to be consistent with coexistence and a spread in the values of T_c between grains.

Acknowlegements We would like to thank Kenton Hammonds (Cambridge) for the symmetry analysis of Table 2, Andrew Ridgwell (Cambridge and UEA) for help with the IR experiments, and Hugh Vass and Wilson Poon (Edinburgh) for the Raman experiments. Computer support was provided in part from a grant awarded by the Royal Society (UK).

References

Alpert NL, Keiser W, Szymanski HA (1970) Theoretical considerations in infrared spectroscopy In: Alpert NL, Keiser W, Szymanski HA (eds) IR: theory and practice of infrared spectroscopy, Chap. 4, 2nd. Plenum, New York

Bates JB (1972) Raman spectra of α and β cristobalite. J Chem Phys 57: 4042–4047

Bradley CJ, Cracknell AP (1972) The mathematical theory of symmetry in solids. Clarendon, Oxford.

Cherukuri SC, Pye LD, Chakraborty IN, Condrate Sr. RA, Ferraro JR, Cornilsen BC, Martin K (1985) The vibrational spectra and normal co-ordinate analysis of ^{28}Si- and ^{29}Si-substituted α-cristobalite. Spectr Lett 18: 123–137

Dolino G, Berge B, Vallade M, Moussa F (1992) Journal de Physique I. Origin of the incommensurate phase of quartz. 1. Inelastic neutron scattering study of the high-temperature β-phase of quartz. Vol. 2, pp 1461–1480

Dove MT (1993) Chapter 8: Anharmonic effects and phase transitions. In: Putnis A, Liebermann RC (eds) Introduction to lattice dynamics. Cambridge topics in mineral physics and chemistry, Chap. 8. Cambridge University Press, Cambridge

Dove MT, Giddy AP, Heine V (1992) On the application of mean-field and Landau theory to displacive phase transitions. Ferroelectrics 136: 33–49

Dove MT, Giddy AP, Heine V (1993) Rigid-unit mode model of displacive phase transitions in framework silicates. Trans Am Crystallogr Assoc 27: 65–75

Dove MT, Heine V, Hammonds KD (1995) Rigid unit modes in framework silicates. Mineral Mag 59: 629–639

Dove MT, Craig MS, Keen DA, Marshall WG, Redfern SAT, Trachenko KO, Tucker MG. (2000) Crystal structure of the high-pressure monoclinic phase-II of cristobalite, SiO_2. Mineral Mag 64: 569–576

Etchepare J, Merian M, Kaplan P (1978) Vibrational normal modes of SiO_2. II. Cristobalite and tridymite. J Chem Phys 68: 1531–1537

Ewen PJS, Dove MT (1983) Raman scattering study of the phase transition in *s*-triazine. Philos Mag (B)47: 641–654

Fateley WG, Dollish FR, McDevitt NT, Bentley FF (1972) Infrared and Raman selection rules for molecular and lattice vibrations: the correlation method. Wiley, New York

Finnie KS, Thompson JG, Withers RL (1994) Phase transitions in cristobalite and related structures by variable temperature infra-red emission spectroscopy. J Phys Chem Solids 55: 23–29

Gaskell PH (1967) The vibrational spectra of silicates. Phys Chem Glasses 8: 69–80

Giddy AP, Dove MT, Pawley GS, Heine V (1993) The determination of rigid-unit modes as potential soft modes for displacive phase transitions in framework crystal structures. Acta Crystallogr (A)49: 697–703

Hammonds KD, Dove MT, Giddy AP, Heine V, Winkler B (1996) Rigid unit phonon modes and structural phase transitions in framework silicates. Am Mineral 81: 1057–1079

Hatch DM, Ghose S, Bjorkstam JL (1994) The α–β transition in AlPO_4 cristobalite: symmetry analysis, domain structure and transition dynamics. Phys Chem Miner 21: 67–77

Hua GL, Welberry TR, Withers RL, Thompson JG (1988) An electron diffraction and lattice dynamical study of the diffuse scattering in β-cristobalite. J Appl Crystallogr 21: 458–465

Hua GL, Welberry TR, Withers RL (1989) Lattice dynamics of α- and β-cristobalite. J Phys Chem Solids 50: 207–213

Krisement O, Trömel G (1959a) Optische Beobachtung der Umwandlung von Cristobalitkristallen und statische Auswertung. Z Naturforsch 14a: 685–686

Krisement O, Trömel G (1959b) Die Umwandlung des Cristobalits. Z Naturforsch 14a: 912–919

Mulliken RS (1933) Electronic structures of ployatomic molecules and valence. IV. Electronic states, quantum theory of the double bond. Phys Rev 43: 279–301

Nord GL (1994) Transformation-induced twin boundaries in minerals. Phase Transit 48: 107–134

Palmer DC, Hemley RJ, Prewitt CT (1994) Raman spectroscopic study of high-pressure phase transitions in cristobalite. Phys Chem Miner 21: 481–488

Petzelt J, Dvorak V (1976a) Changes of infrared and Raman spectra induced by structural phase transitions: I. General considerations. J Phys (C)9: 1571–1586

Petzelt J, Dvorak V (1976b) Changes of infrared and Raman spectra induced by structural phase transitions: II. Examples. J Phys (C)9: 1586–1601

Phillips BL, Thompson JG, Xiao Y, Kirkpatrick RJ (1993) Constraints on the Structure and Dynamics of the β-cristobalite polymorphs of SiO_2 and $AlPO_4$ from ^{31}P, ^{27}Al and ^{29}Si NMR Spectroscopy to 770 K. Phys Chem Miner 20: 341–352

Plendl JN, Mansur LC, Hadni A, Brehat F, Henry P, Morlot G, Naudin F, Strimer P (1967) Low-temperature far-infrared spectra of SiO_2 polymorphs. J Phys Chem Solids 28: 1589–1597

Pryde AKA, Hammonds KD, Dove MT, Heine V, Gale JD, Warren MC (1996) Origin of the negative thermal expansion in ZrW_2O_8 and ZrV_2O_7. J Phys: Condens Matter 8: 10973–10982

Rae AIM (1982) The structural change in *s*-triazine–the quasi-harmonic approximation. J Phys (C) Solid State 15: 1883–1896

Salje EKH (1992) Hard mode spectroscopy: experimental studies of structural phase transitions. Phase Transit 37: 83–100

Salje EKH, Ridgwell A, Güttler B, Wruck B, Dove MT, Dolino G (1992) On the displacive character of the phase transition in quartz: a hard-mode spectroscopy study. J Phys (C)4: 571–577

Sanders MJ, Leslie M, Catlow CRA (1984) Interatomic potentials for SiO_2. Chem Commun 1271–73

Schmahl WW (1993) Athermal transformation behaviour and thermal hysteresis at the SiO_2 α/β cristobalite phase transition. Eur J Mineral, 5: 377–380

Schmahl WW, Swainson IP, Dove MT, Graeme-Barber A (1992). Landau free energy and order parameter behaviour of the α/β phase transition in cristobalite. Z Kristallogr 201: 125–145

Scott JF (1968) Evidence of coupling between one- and two-phonon excitations in quartz. Phys Rev Lett 21: 907–910

Shapiro SM, O'Shea DC, Cummins HZ (1967) Raman scattering study of the α–β-phase transition in quartz. Phys Rev Lett 19: 361–364

Sigaev VN, Smelyanskaya EN, Plotnichenko VG, Koltashev VV, Volkov AA, Pernice P. (1999) Low-frequency band at 50 cm^{-1} in the Raman spectrum of cristobalite: identification of similar structural motifs in glasses and crystals of similar composition. J Non-Cryst Solids 248: 141–146

Simon I, McMahon HO (1953) Study of quartz, cristobalite and vitreous silica by reflection in infrared. J Chem Phys, 21: 23–30

Sosman RB (1965) The phases of silica. Rutgers University Press, New Brunswick, New Jersey

Spearing DR, Farnan I, Stebbins JF (1992) Dynamics of the α–β phase transitions in quartz and cristobalite as observed by in-situ high temperature ^{29}Si and ^{17}O NMR. Phys Chem Miner 19: 307–321

Swainson IP, Dove MT (1993a) Low-frequency floppy modes in β-cristobalite. Phys Rev Lett 71: 193–196

Swainson IP, Dove MT (1993b) Comment on "First-principles studies on structural properties of β-cristobalite". Phys Rev Lett 71: 3610

Swainson IP, Dove MT (1995) Molecular dynamics simulation of α- and β-cristobalite. J Phys Condens Matter 7: 1771–1788

Tautz FS, Heine V, Dove MT, Chen X (1991) Rigid unit modes in the molecular dynamics simulation of quartz and the incommensurate phase transition. Phys Chem Miner 18: 326–336

Thorpe MF (1983) Continuous deformations in random networks. J Non-Cryst Solids 57: 355–370

Vallade M, Berge B, Dolino G (1992) Journal de Physique I. Origin of the incommensurate phase of quartz. 2. Interpretation of inelastic neutron scattering data. Vol. 2, pp 1481–1495

Warren JL, Worlton TG (1974) Improved version of group-theoretical analysis of lattice dynamics Comput phys Commun 8: 71–84

Welberry TR, Hua GL, Withers RL (1989) An optical transform and Monte Carlo study of the disorder in β-cristobalite SiO_2. J Appl Crystallogr 22: 87–95

Withers RL, Thompson JG, Welberry TR (1989) The structure and microstructure of α-cristobalite and its relationship to β-cristobalite. Phys Chem Miner 16: 517–523

Zak J (1969) The irreducible representations of space groups. WA Benjamin, Inc., New York